Structural properties of InAs nanocrystals formed by sequential implantation of In and As ions in the Si (100) matrix

A. Tchebotareva, J. L. Brebner,[a)] and S. Roorda[b)]
*Département de Physique et Groupe de Recherche en Physique et Technologie des Couches Minces,
Université de Montréal, P.O. Box 6128, Station Centre-Ville, Montréal, Québec H3C 3J7, Canada*

P. Desjardins
*Département de Physique et Groupe de Recherche en Physique et Technologie des Couches Minces, École
Polytechnique de Montréal, P.O. Box 6079, Station Centre-Ville, Montréal, Québec H3C 3A7, Canada*

C. W. White
Solid State Division, Oak Ridge National Laboratory, P.O. Box 2008, Oak Ridge, Tennessee 37831-6057

The structural properties of InAs nanocrystals formed in Si by sequential implantation of In and As ions are studied in detail. We use a combination of x-ray diffraction, Rutherford backscattering spectroscopy, channeling, and transmission electron microscopy analyses to demonstrate that, regardless of the order in which ion species are implanted, InAs nanocrystals can be produced in Si (100) by means of sequential ion implantation complemented by subsequent thermal annealing. Whichever the order of implantation is, the nanocrystals are facetted and terminated by (111) planes, the epitaxial relationship being cube-on-cube, $(100)_{InAs} \| (100)_{Si}$ with $[001]_{InAs} \| [001]_{Si}$, for most InAs nanocrystals. The size distribution of nanocrystals is much affected by the sequence of implantation. With As ions implanted first, nanocrystals of different sizes are concentrated within one and the same layer under the sample's surface. In contrast, when In ions are implanted first, nanocrystals of different sizes are produced separately in space, forming a three-layer structure. As a consequence, inverting the order of implantation entails considerable changes in the morphology of the InAs nanocrystals obtained, affecting both their concentration profile and their size distribution. The result has a significant impact on the optical properties of the resulting samples. © *2002 American Institute of Physics.* [DOI: 10.1063/1.1507822]

I. INTRODUCTION

Semiconductor nanocrystals have been intensely studied during the last decade because of their remarkable optical properties arising from quantum confinement effects, and in view of their potential for the design of optoelectronic devices. Various techniques for the synthesis of nanocrystals have been developed, including colloidal chemistry, molecular beam epitaxy, electrochemical etching, and ion implantation (see Ref. 1 and references therein). The use of ion implantation complemented by subsequent thermal annealing[2–18] is especially attractive from the viewpoint of prospective applications because it provides a convenient way to create various types of nanocrystals inside different amorphous and crystalline substrates. In addition to preparing nanocrystals of single-element semiconductors, such as Si and Ge,[5–14] the ion implantation technique also enables one to produce nanocrystals of various II–IV and III–V compound semiconductors. In this way, CdS, CdSe, GaAs, InAs, GaP, InP, and GaN nanocrystals, among others, have been successfully synthesized in silica glasses, sapphire, and crystalline Si substrates.[2–4,11,15–18] However, the morphology of resulting nanocrystals, and the impact of the order of implantation of ion species on the nanocrystalline structure properties have not been previously discussed in the literature, except for Refs. 17 and 19. White *et al.*[17] were the first to point out significant differences in the microstructure of GaAs nanocrystals in Si which arise under the effect of the inversion of the order of implantation. The same effect was observed in Ref. 19 with respect to InAs nanocrystals in Si, and the order of implantation was shown to strongly affect optical properties of the samples.

Hence a significant advantage of the ion implantation lies in its potential for creating nanocrystals with controlled size distributions, and even for producing prescribed nanocrystalline microstructures inside given substrates. Achieving such control is of particular technological importance because it opens new ways of tuning the optical absorption and luminescence–emission wavelengths used in optoelectronic devices. It is therefore essential to understand and control the nucleation and growth of precipitates in ion-implanted materials.

The present article investigates structural properties of InAs nanocrystals synthesized in crystalline Si (100) by sequential implantation of In and As ions followed by thermal annealing. It is demonstrated that the order in which ion species are implanted has a significant impact on the formation of InAs precipitates, and so it strongly affects the morphology of the obtained samples.

[a)]Deceased.
[b)]Author to whom correspondence should be addressed; electronic mail: sjoerd.roorda@umontreal.ca

II. EXPERIMENTAL PROCEDURE

Single-crystalline Si (100) samples were implanted with 800 keV In^+ and 500 keV As^+ ions. The projected ranges for ions of these energies are $R_p(In^+) = 318$ nm and $R_p(As^+) = 310$ nm, with the longitudinal straggling values of $\Delta R_p(In^+) = 60$ nm, and $\Delta R_p(As^+) = 71$ nm. Therefore one could expect the concentration profiles of these two ions to be centered at about the same depth. For each type of ion, the dose implanted was $10^{17}/cm^2$. In each case, the implantation was carried out at $T = 500\,^\circ C$ so as to better preserve the crystallinity of the substrate (epitaxial recrystallization of amorphous Si during its irradiation by an ion beam occurs at temperatures as low as $200\,^\circ C$.)[20]

Two kinds of samples were prepared. Samples of the first kind, to be identified as Si/AsIn further on, were implanted with As^+ ions first and then with In^+ ions. In the second kind of sample, to be referred to as Si/InAs, the order of implantation of the two ion species was inverted. Once implanted, the samples were annealed in a reducing atmosphere ($Ar^+ + 4\% H_2$) at $800\,^\circ C$ for 1 h and then at $900\,^\circ C$ for an additional 1 h.

The microstructure and stoichiometry of both as-implanted and annealed samples were studied using a combination of Rutherford backscattering spectroscopy (RBS), channeling, x-ray diffraction (XRD), as well as cross-sectional transmission electron microscopy (XTEM). The RBS and channeling probe beam consisted of 2 MeV He^+ ions, and all of the spectra were recorded with a detector set at a scattering angle of 170°. In the RBS measurements, the beam was incident at an angle of 7° with respect to the normal of the sample's surface. The spectra obtained were analyzed by means of the RUMP simulation program.[21]

The XRD θ–2θ and rocking curves (with θ the Bragg angle) were obtained using Cu K_α radiation. XTEM specimens were prepared in cross section with $[1\bar{1}0]$ surface normals by conventional mechanical polishing followed by room-temperature low-angle (4°) Ar ion milling at 5 keV in a Gatan precision ion polishing system. The ion energy was gradually reduced during the final stages of thinning in order to minimize sample damage. XTEM images were recorded at 300 kV on a Philips CM30 microscope.

III. RESULTS

A. X-ray diffraction

The XRD measurements were performed on both kinds of samples, first in the as-implanted state, and then after annealing. The obtained curves are shown in Figs. 1(a) and 1(b). Besides the Si(400) substrate peak, the curves for both of the as-implanted samples displayed several crystalline In peaks [Fig. 1(a)]. However, whereas the XRD curve of the Si/AsIn sample did not reveal any peak attributable to crystalline InAs, a low-intensity InAs(200) peak was detected in the corresponding curve of Si/InAs sample near $2\theta = 29.9°$.

Figure 1(b) shows XRD curves for the same samples after annealing. Both Si/AsIn and Si/InAs now display distinct (400) and (200) crystalline InAs peaks, whereas the In peaks have nearly disappeared. Only the In (200) peak remains, although its intensity is greatly reduced. This indi-
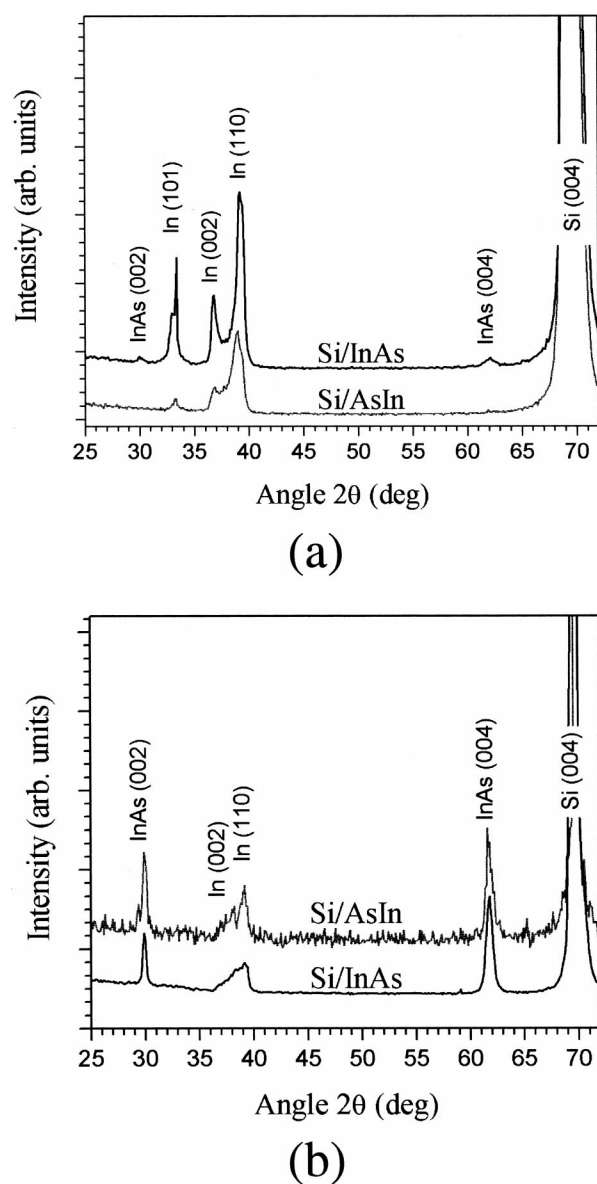

FIG. 1. The XRD diffraction patterns of the samples: (a) as-implanted state and (b) after the annealing (1 h at 800 °C followed by 1 h at 900 °C).

cates that in both types of samples, after annealing, most of the In is present in the form of crystalline InAs.

The widths of the InAs (400) peaks, as determined from high-resolution XRD by use of Cu $K_{\alpha 1}$ radiation (not shown here), are 0.35° for the Si/AsIn sample and 0.36° for the Si/InAs one. The average size D of nanocrystals can be evaluated from the line broadening due to the finite crystal size using the Scherrer formula

$$D = \frac{0.9\lambda}{B \cos \theta_B}, \tag{1}$$

where B is the line broadening due to the finite (small) crystal size, λ is the x-ray wavelength, and θ_B is the corresponding Bragg angle. From Eq. (1) we obtain nanocrystal diameters of about 23 nm for the Si/AsIn sample and 26 nm for the Si/InAs one.
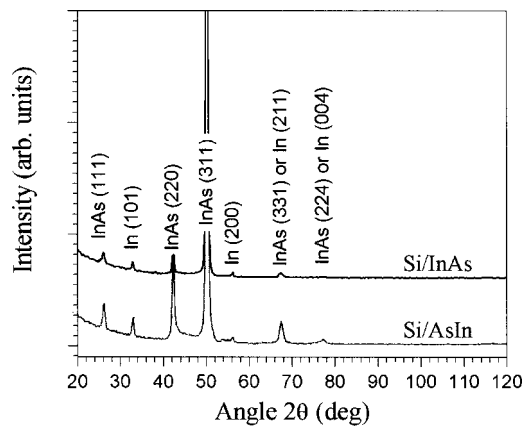
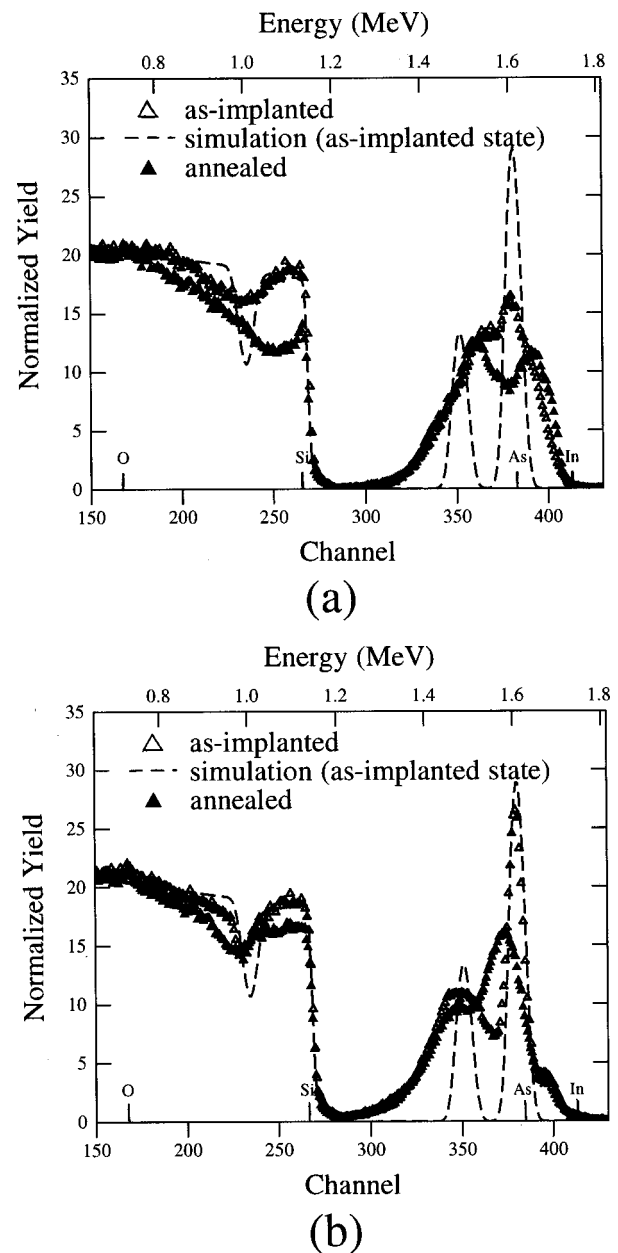FIG. 2. Grazing-angle XRD curves of the annealed samples.

(a)

(b)

FIG. 3. The RBS spectra of the samples before and after annealing. The dashed vertical lines denote the surface channels of Si, As, and In atoms: (a) Si/AsIn sample and (b) Si/InAs sample.

Grazing-incidence XRD measurements, with the x-ray beam angle of incidence being fixed while the detector is scanned, were carried out on annealed samples to determine the orientation of the nanocrystals. The angle of incidence was chosen to be about 0.3° so as to fulfill the Bragg condition for the (311) planes in InAs crystals for which the (100) planes are parallel to those of the Si (100) matrix. Figure 2 shows the curves obtained for both kinds of samples. These curves exhibit a strong InAs (311) peak along with several In and InAs peaks of much lower intensity. This, together with selected-area electron diffraction results, establishes the epitaxial relationship between InAs and Si to be cube-on-cube. $(100)_{InAs}\|(100)_{Si}$ with $[001]_{InAs}\|[001]_{Si}$, for most InAs nanocrystals. Quantitative analysis of the integrated peak intensity of the XRD data presented in Fig. 2, with the geometrical structure factor and Lorentz factor taken into account, indicates that the fraction of InAs nanocrystals having orientations different from that of the Si(100) substrate is $10\%\pm0.5\%$ for Si/AsIn and $3\%\pm0.5\%$ for Si/InAs.

B. Ion-beam analysis (RBS) and channeling

Both as-implanted and annealed samples were characterized by RBS. Typical spectra of as-implanted samples are shown in Fig. 3 as open (white) triangles together with the TRIM simulation spectra of Si implanted with In and As ions (dashed lines). The spectrum of Si/InAs reveals a broad peak corresponding to the As ion distribution, as well as a sharp peak corresponding to In ions. The latter indicates a sharp concentration profile of In, as sharp as would be expected based on the range straggling during the implantation. Such a narrow distribution of In after a high-dose ion implantation could indicate segregation of the In ions, and indeed, In crystallites were detected by XRD and transmission electron microscope (TEM) measurements. Both In and As distributions appear to be centered at depths close to those predicted by TRIM simulation. The spectrum of the Si/AsIn sample shows two broad peaks attributable to the In and As ion distributions. The In peak is centered at its expected projected range, whereas the center of the As distribution is located closer to the substrate's surface than predicted by TRIM. This displacement is likely to be due to the sputter erosion of the surface of As ion-implanted Si substrate by In ions during implanta-

tion. Hence, there is a considerable difference between the RBS spectra of the Si/AsIn and Si/InAs samples immediately after ion implantation.

The depth distributions of the In and As ions (not shown here) were extracted from these spectra, as well as from other spectra recorded at different scattering angles. Significant deviations from the standard implantation profile were observed, as could be expected for such high-dose heavy ion implants. Specifically, the widths of As ion distributions in both samples are much greater than the corresponding values of straggling predicted by TRIM simulation, as shown in Fig. 3. The same is true for the distribution of In ions in Si/AsIn sample. By contrast, the width of In distribution in the Si/InAs sample corresponds to the one predicted by TRIM (see Fig. 3). However, most of the implanted species were con-

fined to a 500 nm thick surface layer with partial overlap between the As and In profiles in the as-implanted samples [see Figs. 3(a) and 3(b)].

Black triangles in Fig. 3 represent the spectra measured after the thermal anneal treatment. In these spectra, the energy difference between the As and In peaks corresponds exactly to that between the As and In surface channels, which indicates that the overlap of the depth profiles of these species is significantly increased as compared to the as-implanted state. Such an increase in the overlap would result if an InAs compound had formed. However, in both samples the width of the As distribution is still greater than that of the In distribution, indicating that a fraction of implanted ions still remains in the substrate in a form other than molecular or crystalline InAs.

The microstructure of the annealed samples was also investigated by channeling the 2 MeV He$^+$ ion beam along the [001], [011], and [111] crystallographic directions of the Si(100) substrate. The spectra obtained for the [001] direction in both Si/AsIn and Si/InAs are presented in Figs. 4(a) and 4(b). For each sample, the channeled spectrum (black triangles) is shown together with the corresponding random spectrum (solid line). The spectra show a reduction of the backscattering yield for all channels in both samples demonstrating very clearly that they are crystalline. The minimum yield, however, is about three times greater than in unimplanted Si wafers, which suggests the presence of a considerable number of defects resulting from ion implantation. The yield is also reduced between channels 300 and 450, corresponding to backscattering from As and In, although the reduction is somewhat less than in the substrate.

The ratios of the channeling yield in the channel range 300–450 (In and As signal) to the channeling yield for the channels 100–280 (Si signal), designated by χ_{As+In}/χ_{Si} and χ_{In+As}/χ_{Si} for Si/AsIn and Si/InAs samples, respectively, were calculated from channeling spectra measured in [001], [011], and [111] directions of silicon substrate. These ratios remain constant for all the three directions in each kind of sample, indicating that a large fraction of In and As atoms are aligned along the same crystallographic axes as the Si substrate. This result is consistent with the formation of InAs crystallites embedded epitaxially within the Si matrix.

A higher channeling yield from the InAs portions of the spectra (as compared to the yield from the Si range) can be attributed to a number of structural imperfections. Specifically, some of the In and As atoms may remain in solution on nonsubstitutional sites, some of the InAs crystallites may have formed but still not aligned epitaxially with the Si matrix, and some larger InAs crystallites may have relaxed toward their normal lattice parameter. It is also possible that dislocations and other types of extended defects are formed inside these nanocrystals.

C. Transmission electron microscopy

The TEM measurements were carried out on both Si/AsIn and Si/InAs samples, before and after thermal annealing. The micrographs of the as-implanted samples are shown in Fig. 5. The dark spots and agglomerates of different sizes,
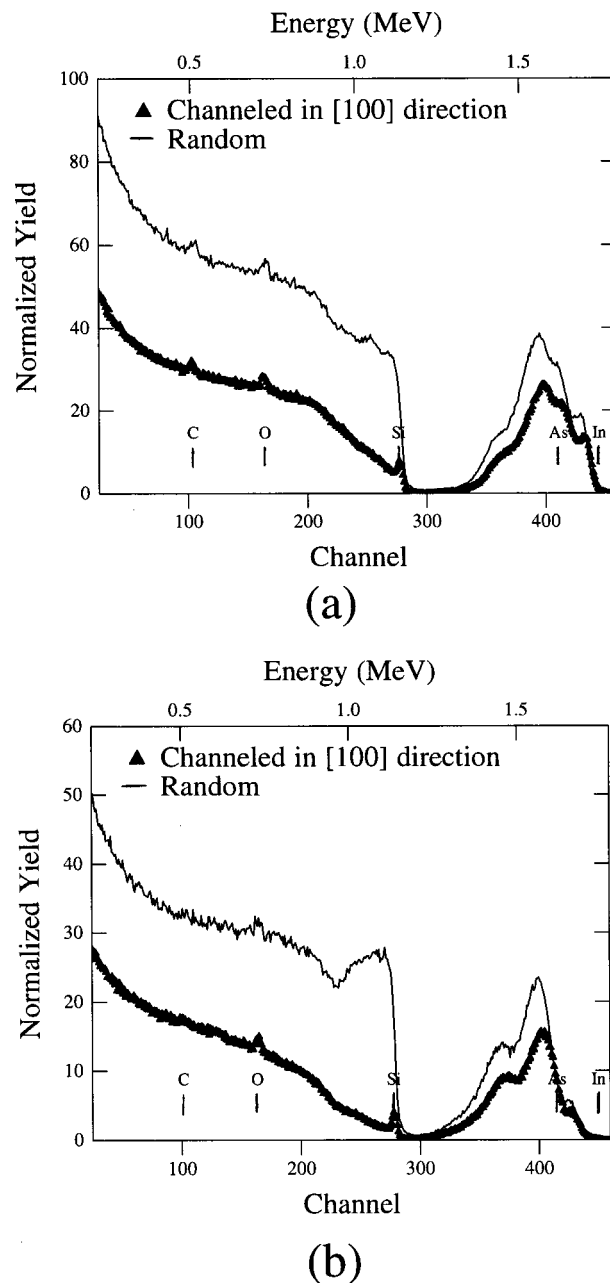

FIG. 4. Channeling spectra measured in [001] silicon matrix direction: (a) Si/AsIn sample and (b) Si/InAs sample.

located at depths greater than the projected range R_p (about 310 nm), have been identified by XRD analysis as indium nanocrystals. With In ions implanted first (panel b), some of these nanocrystals have the shape of platelets in the plane normal to the implantation direction (they appear as wires in the two-dimensional projection of the cross-sectional TEM images) and are considerably larger than in the case of As ions implanted first (panel a). In both cases these nanocrystals are confined to a 650 nm thick surface layer. The largest of these nanocrystals are located at a depth corresponding to the projected range R_p as predicted by TRIM for the implanted In ions. The formation of smaller nanocrystals at larger depths would require diffusion during ion implantation.
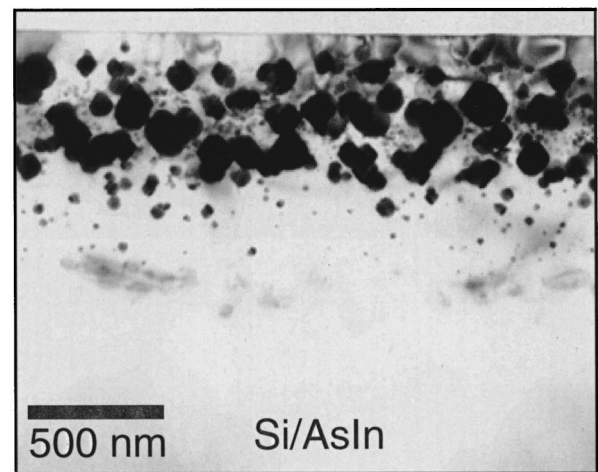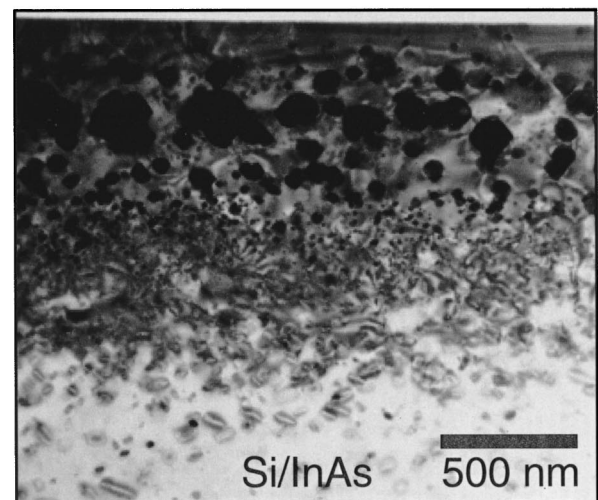
FIG. 6. XTEM micrographs of samples after annealing: (a) Si/AsIn and (b) Si/InAs.
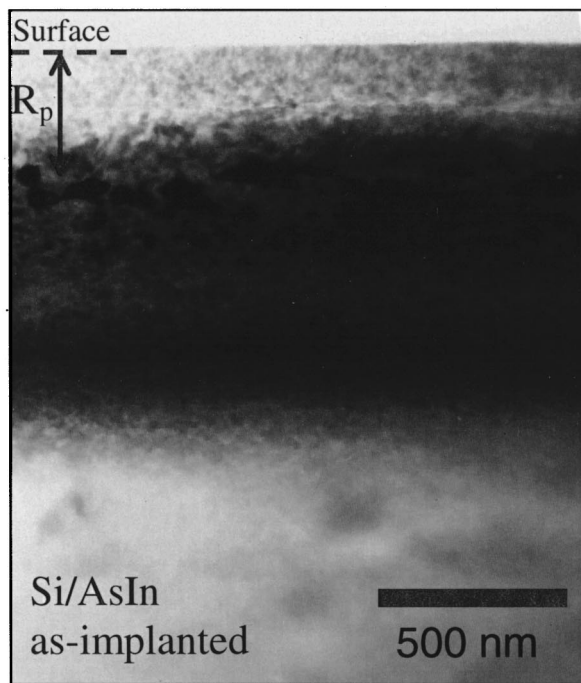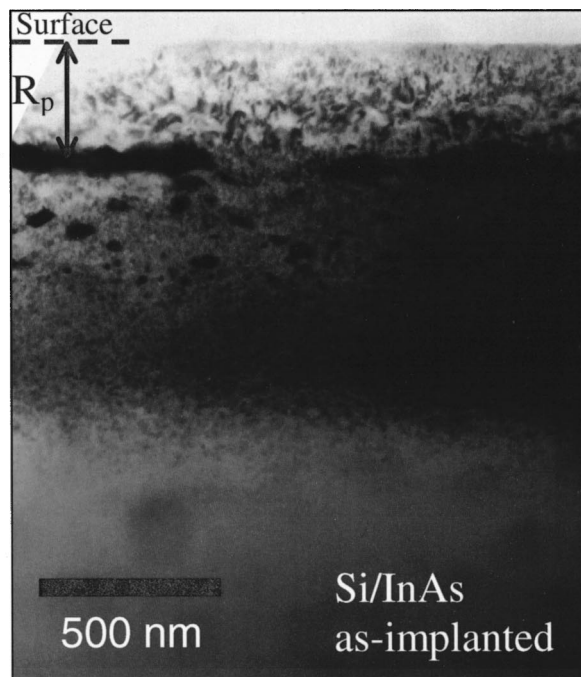
FIG. 5. XTEM micrographs of samples in as-implanted state: (a) Si/AsIn and (b) Si/InAs.

of nanocrystals form sets of parallel planes aligned at an angle of 54.7° with respect to the substrate's surface and hence are identified to be {111} planes, in agreement with the epitaxial relationship that was obtained from grazing-angle XRD.

It is worth noting that a large number of extended defects are formed in the Si/InAs sample after annealing, but not in the Si/AsIn sample. Dislocations and dislocation loops are created in Si/InAs far beyond the projected range of the implanted ions. A number of dislocations is also seen between the sample's surface and the layer containing InAs nanocrystals. These defects are likely to cause nonradiative carrier recombination during a photoluminescence (PL) excitation and thus prevent PL emission from the sample.[19]

D. Size distribution

We performed a quantitative analysis of the TEM images, such as those in Fig. 6, to obtain the size and depth distribution of the InAs nanocrystals. A total of 287 nano-

The TEM micrographs of annealed Si/AsIn and Si/InAs samples shown in Figs. 6(a) and 6(b) demonstrate that the annealing resulted in the formation of InAs nanocrystals in both kinds of samples. From the shape of dark spots in these micrographs it becomes clear that nanocrystals obtained in the samples of both kinds are facetted. Moreover, the facets

crystals of more than 10 nm in diameter were taken into account for the Si/AsIn sample, whereas 484 nanocrystals were considered for Si/InAs. The average diameter of the nano-crystals, evaluated without regard to the depth of their location, was found to be 58.3 nm for Si/AsIn sample and 28.0 nm for Si/InAs. The difference is due to a large number of nanocrystals with small diameters (less than 25 nm) that are present in Si/InAs at depths exceeding 600 nm. In both samples, the average size of nanocrystals is larger than that obtained from XRD analyses. Indeed, the calculations from TEM micrographs are referred to as nanocrystals of discernible sizes alone, whereas XRD analysis is sensitive to nanocrystals of all sizes actually present. Correspondingly, the line broadening supplied by XRD analysis is affected by all of the nanocrystals existing in the sample. As a result, the TEM analysis tends to overestimate the average size of the nanocrystals obtained. However, in the case of the Si/InAs sample the agreement between the nanocrystal's average diameters evaluated from high resolution XRD and TEM measurements, turns out to be good, due to the large number of small nanocrystals that are visible on the micrographs.

Distributions of the average diameter D of nanocrystals as a function of depth are shown in Figs. 7(a) and 7(b). For the Si/AsIn sample, D is a slowly varying function of depth. Moreover, at every fixed depth the average diameter is proportional to the concentration of implanted ions and has a one-layer structure. In other words, in the Si/AsIn sample nanocrystals of different sizes are concentrated within one and the same layer under the sample's surface. By contrast, in the Si/InAs sample the depth distribution of the average size has a three-layer structure. In this sample the layer containing large nanocrystals lies at a depth of about 300–400 nm. This layer is surrounded on either side by a layer with nanocrystals of considerably smaller size [Fig. 6(b)]. A careful examination of an enlarged version of the XTEM image in Fig. 6(b) reveals that only a small number of nanocrystals have their centers lying in the regions adjacent to the layer of large nanocrystals, their depths extending from 200 to 300 nm, and from 400 to 500 nm. Such a layered structure is characteristic of a precipitation process dominated by Oswald's ripening.[22] Hence, for the Si/InAs sample the probability of finding a nanocrystal of a given size is strongly dependent on the depth of the nanocrystal's location under the sample's surface. This fact is also illustrated in Figs. 8(a) and 8(b) which display the depth distributions of very small nanocrystals (less than 29 nm in diameter), and of very large ones (greater than 69 nm in diameter), respectively.

Consequently, in the case of the Si/AsIn sample, nanocrystals of different sizes are formed with the same probability at every depth where the process of synthesis is efficient. By contrast, in the case of the Si/InAs sample, nanocrystals of all sizes are formed with nearly the same probability only at depths smaller than 650 nm, whereas for depths between 650 and 960 nm the formation of very small nanocrystals (those with diameter lesser than 29 nm) is favored. As a result, in Si/InAs the distribution of the sizes of nanocrystals over depth is multimodal.
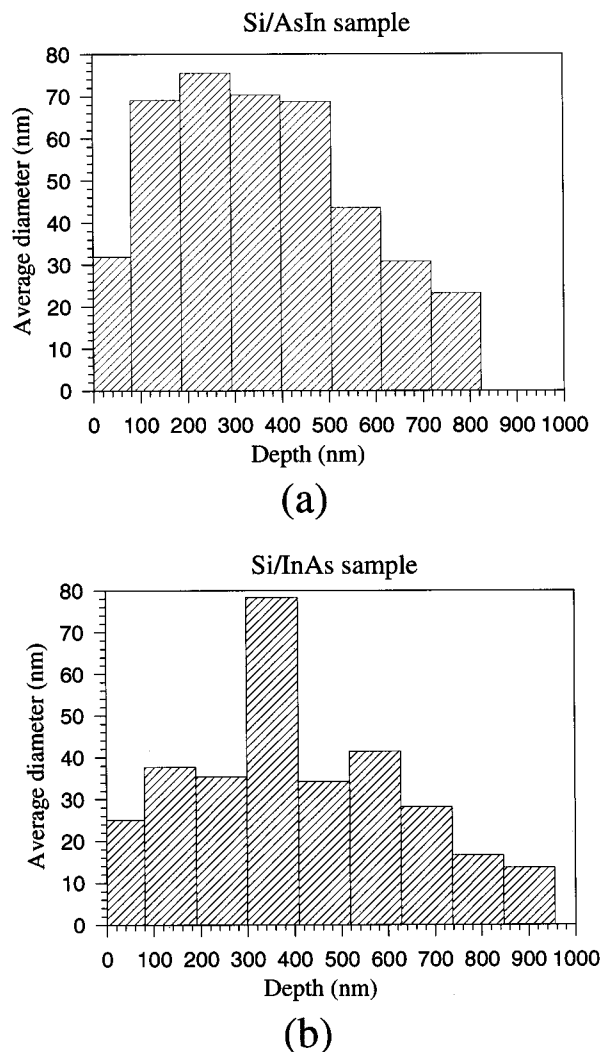

FIG. 7. Average size of nanocrystals as a function of depth under the sample's surface: (a) Si/AsIn and (b) Si/InAs.

IV. DISCUSSION

All of the results we have obtained by means of structural analysis reveal a considerable structural difference between Si/AsIn and Si/InAs samples. Based on the total set of the results, we propose the following phenomenological model for the formation of InAs nanocrystals in Si (100) created by ion implantation at 500 °C followed by subsequent thermal annealing. The equilibrium solubility of As in Si is considerably higher than that of In (2.5×10^{20} cm^{-3} for As atoms versus 4.0×10^{18} cm^{-3} for In atoms at $T = 900$ °C). Even though the conditions in our experiment are far from equilibrium, our observations (In nanocrystals but no As segregation) indicate that the system follows a trend similar to that of the equilibrium system. Moreover, the formation of relatively stable vacancy–As complexes (V–As$_3$) at high As concentration and high temperature[23] prevents As segregation. Hence, when As is implanted first, it tends to remain essentially atomically dispersed. When In ions are added afterward, some of them are involved in the formation of InAs, which remains in molecular form in the substrate (this step in the process may be enhanced by the affinity of In for the vacancy in the V–As$_3$ complexes). The remainder
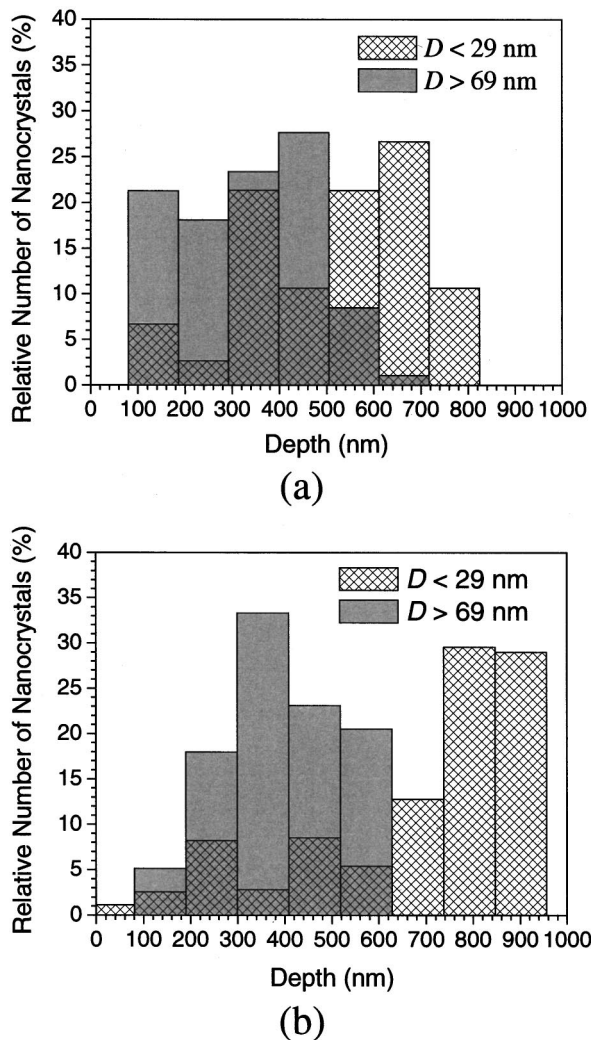
FIG. 8. Layered structure of the size distribution of InAs nanocrystals: (a) Si/AsIn and (b) Si/InAs.

V. CONCLUSIONS

The structural measurements performed by use of various experimental techniques as described above demonstrated the possibility of producing InAs nanocrystals in Si (100) by means of sequential ion implantation complemented by subsequent thermal annealing, regardless of the order in which ion species are implanted. Whichever the sequence of implantation is, the nanocrystals produced are terminated by (111) facets while being epitaxial with the Si(100) substrate. We find, however, that inversion in the implantation sequence strongly affects the distribution of nanocrystals' sizes over depth. When As is implanted first, nanocrystals of difference sizes are concentrated within one and the same layer under the sample's surface. By contrast, implantation of In followed by As results in nanocrystals of different sizes being located separately in space. This has an appreciable effect on the optical properties of the resulting samples, as was reported in Ref. 19.

of the implanted In ions, due to their low solubility in Si, experience diffusion and segregate in In nanocrystals. These nanocrystals are clearly seen in XRD measurements and TEM micrographs. By contrast, when In ions are implanted first, they tend to diffuse in the course of implantation, then segregate in the form of In nanocrystallites. In this case, nanocrystals of In obtained after the end of implantation are much larger than those obtained in the case of As implanted first, which can be seen from the TEM results of Figs. 7(a) and 7(b). A small fraction of In ions remain in solution in Si. When As ions are added afterward, these In ions are converted into InAs compound in molecular form. During the anneal, the InAs compound, which is present in molecular form in the samples of both kinds, segregates in InAs nanocrystals. The In nanocrystals existing in the samples of both kinds melt during the anneal, and the In atoms diffuse in the sample. Part of them form a nanocrystalline InAs compound with the implanted As ions, while the other part segregates once again in In nanocrystals. Thus, after annealing both InAs nanocrystals and In nanocrystals are present in the samples.

[1] See, for example, J. Lumin. **70**, (1996), special issue, *Spectroscopy of Isolated and Assembled Semiconductor Nanocrystals*, edited by L. E. Brus, A. L. Efros, and T. Itoh.
[2] P. Madakson, E. Ganin, and J. Karasinski, J. Appl. Phys. **67**, 4053 (1990).
[3] S. Yu. Shiryaev, A. Nylandsted Larsen, and M. Deicher, J. Appl. Phys. **72**, 410 (1994).
[4] S. Yu. Shiryaev and A. Nylandsted Larsen, Nucl. Instrum. Methods Phys. Res. B **80/81**, 846 (1992).
[5] H. Atwater, K. V. Shcheglov, S. S. Wong, K. J. Vahala, R. C. Flagan, M. L. Brongersma, and A. Polman, Mater. Res. Soc. Symp. Proc. **316**, 409 (1994).
[6] T. Shimizu-Iwayama, K. Fujita, S. Nakao, K. Saitoh, T. Fujita, and N. Itoh, J. Appl. Phys. **75**, 7779 (1994).
[7] J. G. Zhu, C. W. White, J. D. Budai, S. P. Withrow, and Y. Chen, Mater. Res. Soc. Symp. Proc. **358**, 175 (1995).
[8] J. G. Zhu, C. W. White, J. D. Budai, S. P. Withrow, and Y. Chen, J. Appl. Phys. **77**, 4386 (1995).
[9] K. S. Min, K. Y. Shcheglov, C. M. Yang, H. A. Atwater, M. L. Brongersma, and A. Polman, Appl. Phys. Lett. **68**, 2511 (1996).
[10] W. Skorupa, R. A. Yankov, I. E. Tyschenko, H. Frob, T. Bohme, and K. Leo, Appl. Phys. Lett. **68**, 2410 (1996).
[11] C. W. White, J. D. Budai, J. G. Zhu, S. P. Withrow, D. M. Hembree, D. O. Henderson, A. Ueda, Y. S. Tung, and R. Mu, Mater. Res. Soc. Symp. Proc. **396**, 377 (1996).
[12] K. S. Min, K. V. Shcheglov, C. M. Yang, H. A. Atwater, M. L. Brongersma, and A. Polman, Appl. Phys. Lett. **69**, 2033 (1996).
[13] P. Mutti, G. Ghislotti, S. Bertoni, L. Bonoldi, G. F. Cerofolini, L. Meda, E. Grilli, and M. Guzzi, Appl. Phys. Lett. **66**, 851 (1995).
[14] C. W. White, J. D. Budai, J. G. Zhu, S. P. Withrow, S. J. Pennycook, D. M. Hembree, D. S. Zhou, T. Yo-Dihn, and R. H. Magruder, Mater. Res. Soc. Symp. Proc. **316**, 487 (1994).

[15] C. W. White *et al.*, J. Appl. Phys. **79**, 1876 (1996).

[16] R. H. Magruder, J. E. Witting, and R. A. Zuhr, J. Non-Cryst. Solids **163**, 162 (1993).

[17] C. W. White *et al.*, J. Nucl. Instrum. Methods Phys. Res. B **127/128**, 545 (1997).

[18] J. A. Wolk, K. M. Yu, E. D. Bourret-Courchesne, and E. Johnson, Appl. Phys. Lett. **70**, 2268 (1997).

[19] A. L. Tchebotareva, J. L. Brebner, S. Roorda, and C. W. White, Nucl. Instrum. Methods Phys. Res. B **175–177**, 187 (2001).

[20] F. Priolo, C. Spinella, and E. Rimini, Phys. Rev. B **41**, 5235 (1990).

[21] M. Thompson and L. Doolittle, "RUMP-RBS Analysis and Simulation Package," Computer Graphic Service, Ltd., 1988–1997.

[22] V. A. Borodin, K.-H. Heinig, and S. Reiss, Phys. Rev. B **56**, 5332 (1997).

[23] V. Ranki, J. Nissilä, and K. Saarinen, Phys. Rev. Lett. **88**, 105 506 (2000).